Feasibility of external beam radiation therapy to deep-seated targets with kilovoltage x-rays

Magdalena Bazalova-Carter[a)]
Department of Physics and Astronomy, University of Victoria, PO Box 1700 ST CSC, Victoria, BC V8W 2Y2, Canada

Michael D. Weil
Sirius Medicine LLC, Box 414, Half Moon Bay, CA 94019, USA

Dylan Yamabe Breitkreutz
Department of Physics and Astronomy, University of Victoria, PO Box 1700 ST CSC, Victoria, BC V8W 2Y2, Canada

Brian P. Wilfley
Triple Ring Technologies, 39655 Eureka Dr, Newark, CA 94560-4806, USA

Edward E. Graves
Department of Radiation Oncology, Stanford University, 875 Blake Wilbur Dr, Stanford, CA 94305-5847, USA

(Received 7 July 2016; revised 10 November 2016; accepted for publication 14 November 2016; published 30 January 2017)

Purpose: Radiation therapy to deep-seated targets is typically delivered with megavoltage x-ray beams generated by medical linear accelerators or ^{60}Co sources. Here, we used computer simulations to design and optimize a lower energy kilovoltage x-ray source generating acceptable dose distributions to a deep-seated target.

Methods: The kilovoltage arc therapy (KVAT) x-ray source was designed to treat a 4-cm diameter target located at a 10-cm depth in a 40-cm diameter homogeneous cylindrical phantom. These parameters were chosen as an example of a clinical scenario for testing the performance of the kilovoltage source. A Monte Carlo (MC) model of the source was built in the EGSnrc/BEAMnrc code and source parameters, such as beam energy, tungsten anode thickness, beam filtration, number of collimator holes, collimator hole size and thickness, and source extent were varied. Dose to the phantom was calculated in the EGSnrc/DOSXYZnrc code for varying treatment parameters, such as the source-to-axis distance and the treatment arc angle. The quality of dose distributions was quantified by means of target-to-skin ratio and dose output expressed in D_{50} (50% isodose line) for a 30-min irradiation in the homogeneous phantom as well as a lung phantom. Additionally, a patient KVAT dose distribution to a left pararenal lesion (~1.6 cm in diameter) was calculated and compared to a 15 MV volumetric modulated arc therapy (VMAT) plan.

Results: In the design of the KVAT x-ray source, the beam energy, beam filtration, collimator hole size, source-to-isocenter distance, and treatment arc had the largest effect on the source output and the quality of dose distributions. For the 4-cm target at 10-cm depth, the optimized KVAT dose distribution generated a conformal plan with target-to-skin ratio of 5.1 and D_{50} in 30 min of 24.1 Gy in the homogeneous phantom. In the lung phantom, a target-to-skin ratio of 7.5 and D_{50} in 30 min of 25.3 Gy were achieved. High dose conformity of the 200 kV KVAT left pararenal plan was comparable to the 15 MV VMAT plan. The volume irradiated to at least 10% (<240 cGy) of the prescription dose was 2.2 × larger in the 200 kV KVAT plan than in the 15 MV VMAT plan, but considered clinically insignificant.

Conclusions: This study demonstrated that conformal treatments of deep-seated targets were achievable with kilovoltage x-rays with dose distributions comparable to MV beams. However, due to the larger volumes irradiated to clinically tolerated low doses, KVAT x-ray source usage for deep-seated lesions will be further evaluated to determine optimal target size. © *2016 American Association of Physicists in Medicine* [https://doi.org/10.1002/mp.12047]

Key words: kilovoltage photon beams, Monte Carlo, radiation therapy

1. INTRODUCTION

Radiotherapy of deep-seated targets is most commonly delivered with megavoltage (MV) 6–20 MV x-ray beams or ^{60}Co beams.[1] MV x-ray beams, typically generated by medical linear accelerators (linacs), are characterized by a build-up region resulting in lower skin dose and slow dose fall-off in tissue that enable treatments of targets located deep in a patient's body. In a modern linac, electrons are first accelerated in waveguides consisting of precisely manufactured linear arrays of microwave cavities and then converted into x-rays upon interacting with a tungsten anode.[2] Due to the complex design of a linac,

these radiotherapy machines are large, heavy, and expensive. In addition, the highly penetrating nature of MV radiation requires treatment "bunkers" that are custom-built, massive, and expensive. On the other hand, kilovoltage (kV) x-ray beams can be generated in a relatively simple and inexpensive way using x-ray tubes. The drawback of kV beams is their high skin dose and fast fall-off in tissue resulting in difficulties treating deep-seated targets. The goal of this work was to optimize a design of a cost-effective radiotherapy kV x-ray source to overcome these hurdles and to investigate whether it could effectively deliver conformal radiotherapy to a deep-seated target. We estimate the cost of the novel x-ray source to be approximately 10% of the cost of a modern linac.

Conformal kV x-ray beam radiotherapy has recently been studied for partial breast irradiations. Prionas et al.[3] used Monte Carlo (MC) simulations to investigate 178-keV rotational x-ray beam dose distributions in the breast delivered with their dedicated breast computed tomography (bCT) platform. The authors demonstrated that kV x-ray beam conformal doses with high skin sparing could be achieved for a spherical target of 1 cm in size in the center of a 14-cm diameter phantom. Here, we have investigated kV x-ray beam dose distributions for a more challenging case: we have simulated treatments of a larger target deep within two human torso-sized phantoms.

In this work, we built a MC model of a kilovoltage arc therapy (KVAT) x-ray source that was designed *in silico* by modifying the geometry of an existing large-area (23 × 23) cm^2 multi-focal-spot diagnostic kV x-ray source.[4] The original source consisted of a 2D array of 100 × 100 x-ray beamlets generated by an electron beam scanned on a large tungsten anode and shaped by a collimator.[5] We have modified the arrangement of the sources to form a linear array and thoroughly optimized the x-ray source and the collimation system design for the delivery of conformal doses to a 4-cm diameter target at a depth of 10 cm in a 40 cm diameter cylindrical phantom. We have demonstrated the possibility of delivering clinically relevant dose rates of 1 Gy/min with a 200 kV x-ray beam while maintaining an acceptably low dose to the skin.

2. MATERIALS AND METHODS

2.A. KVAT x-ray source design

The imaging source design was modified for delivery of conformal radiotherapy to a 4-cm diameter spherical target at 10-cm depth in a 40-cm diameter cylindrical phantom. We employed this depth in the model to investigate the capabilities of the source for lesions significantly below the skin based on average adult body dimensions.[6] The size of the simulated lesion was selected as an approximation of measurements of common, moderately advanced, but potentially curable tumors, that is, stage T2, lung, breast, and pancreas.[7] While the tungsten anode geometry of the modeled transmission source including the niobium, beryllium, and water layer was maintained, the beam arrangement and the x-ray collimator were modified significantly. First, the x-ray beams were re-arranged from a 2-D array into a linear array and their number was significantly reduced (Fig. 1(a)). Second, in order to produce sharp beams, the collimator thickness was increased from 2 cm to 10 cm. Nine tapered collimator holes of 3-mm diameter at the anode side spread across 50 cm were designed in such a way that all nine x-ray beams just covered the 4-cm diameter spherical target at 10-cm depth for a source-to-axis distance (SAD) of 45 cm. The SAD was defined as the distance from the end of the collimator to the isocenter. Note that the [SAD − 10 cm] corresponded to the clearance between the patient and the x-ray source. A 120° arc treatment with an isocenter coinciding with the center of the target was considered (Fig. 1(b)).

2.B. KVAT x-ray source modeling

The Monte Carlo model of the KVAT source was built in the EGSnrc/BEAMnrc (V4 2.4.0) code.[8,9] The scanning

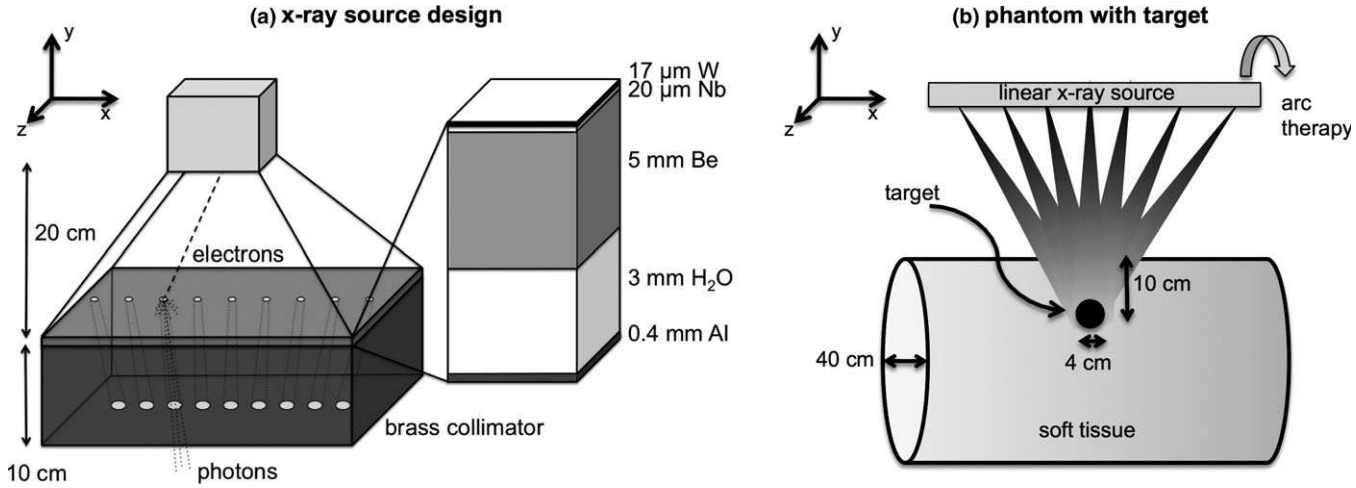

FIG. 1. A schematic drawing of the proposed KVAT x-ray source (a). The x-ray source was designed to treat a 4-cm diameter at 10-cm depth in a 40-cm diameter cylinder using arc therapy (b).

electron beam was simulated as a mono-energetic pencil beam for each collimator hole in a separate simulation. Electrons travelled in vacuum before interacting with the anode placed 20 cm away from the electron source (Fig. 1(a)). The 17-μm tungsten anode, the 20-μm niobium layer, the 5-mm beryllium window, the 3-mm thick water-cooling layer, and the 0.4-mm-thick aluminum filter were simulated using the SLABS component module (CM). Variance reduction techniques were used for the simulation of x-ray generation. Uniform Bremsstrahlung splitting with a splitting factor of 200, as well as tungsten Bremsstrahlung cross-section enhancement with enhancement constant = 1, and enhancement factor = 200[10] were used (both with Russian Roulette on). Both the photon and electron transport cutoff kinetic energies were 10 keV in the anode.

The brass collimator was modeled with 5 layers of the BLOCK CM, within which each collimator hole was simulated as an eight-sided polygon. The photon and electron transport cutoff kinetic energies were 10 keV and 300 keV in the collimator, respectively (i.e., electrons were not transported). Phase-space files for each collimator hole (or beamlet) were scored just below the collimator. All phase-space files contained at least 10^5 particles and were calculated in approximately 12 h on a 2 × 3.06 GHz 6-Core Intel Xeon computer.

2.C. Phantom study

MC KVAT dose was calculated for two cylindrical phantoms in the EGSnrc/DOSXYZnrc code.[11] The dose expressed in Gy per particle was converted into dose delivered in a 30 min irradiation with a 200 mA tube current using a conversion factor of 8.86×10^{20} particles/(30 min/200 mA) calculated by Bazalova et al.[12]

2.C.1. Phantom modeling

First, a cylindrical phantom with a diameter of 40 cm and a length of 20 cm was modeled with a uniform voxel size of $(0.4 \times 0.4 \times 0.4)$ cm^3. MC dose calculations for each beamlet (each collimator hole was represented by a unique phase-space file) were run separately using the phase-space source from multiple directions (ISOURCE=8), which allowed for easy beamlet weighting. The phantom's material was set to ICRU tissue[13] and the surrounding material between the phantom and the phase-space file was set to air. Source-to-isocenter distance was selected according to the SAD assumed in the generation of the phase-space files.

Second, a heterogeneous cylindrical lung phantom of 40 cm in diameter and 20 cm in length was modeled with a uniform voxel size of $(0.2 \times 0.2 \times 0.2)$ cm^3. The lung phantom (its geometry is shown in Fig. 8) contained lungs, ribs, the sternum, the spinal cord, and the heart and was uniform along the cylinder axis (the *x*-axis in Fig. 1). The dimensions of the bony structures and organs were matched to patient data. The compositions and mass densities ρ of the lungs (ρ=0.26 g/cm^3), ribs (ρ=1.42 g/cm^3), and the heart (ρ=1.06 g/cm^3) were modeled according to the ICRU-44 report.[13] Due to the lack of suitable ICRU-44 data, the sternum was modeled as ribs and the spinal cord was modeled as cortical bone (ρ=1.92 g/cm^3). For a direct comparison of lung phantom and homogeneous phantom dose distributions, an equivalent homogeneous cylindrical phantom with $(0.2 \times 0.2 \times 0.2)$ cm^3 voxels was also generated.

2.C.2. Optimization of source and treatment delivery parameters

In order to optimize the dose distribution to the 4-cm diameter target at 10-cm depth in the 40-cm diameter cylindrical homogeneous tissue phantom, the x-ray source parameters were varied and their effect on the quality of dose distributions was investigated. The studied x-ray source parameters are illustrated in the schematic x-ray source drawing in Fig. 2 and their values are summarized in Table I. The effect of electron beam energy, anode thickness, source extent, beam filtration, collimator hole size at the anode side, collimator thickness, number of collimator holes, and source-to-isocenter distance was evaluated. All studied values were chosen as realistic and

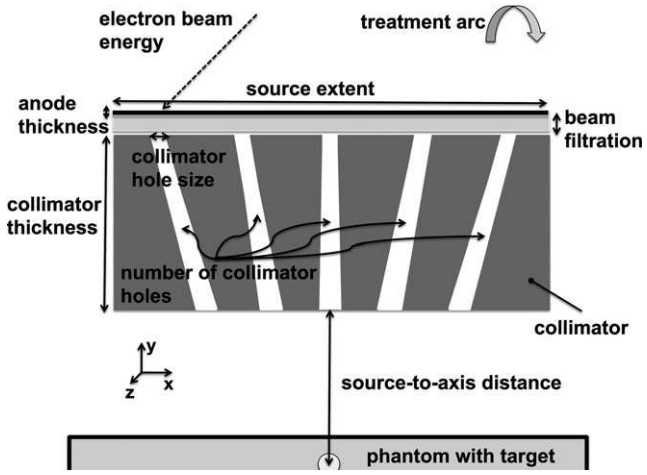

FIG. 2. Treatment source and geometry parameters have been varied to find the optimum setup for treatment of a 4-cm diameter and 10 cm deep target.

TABLE I. The default (in bold) and varied treatment source parameter values. For each investigated parameter, the other parameters were kept at their default values.

Parameter	Values
Electron beam energy (keV)	120, 150, 180, **200**
Anode thickness (μm)	12, **17**, 22, 32
Beam filtration (mm)	**0.4**, 1, 4, 7 **Al** and 1, 2, 3 Cu
Number of collimator holes	7, **9**, 21, 41
Source extent (cm)	30, 40, **50**, 60
Collimator hole size at the anode side (mm)	1, **3**, 5, 7
Collimator thickness (cm)	6, 8, **10**, 12
Source-to-axis distance (cm)	25, 35, **45**, 55, 65
Treatment arc angle (°)	60, 80, **120**, 160, 180

achievable in the design of the KVAT source. A Matlab (The Mathworks, Nattick, MA) code was developed to automatically generate BEAMnrc input files based on the target size and location taking into account the various x-ray source and treatment parameters discussed above.

First, MC dose distributions were calculated for the default set of parameters indicated in bold font in Table I: 200 keV electron beam energy, 17 μm anode thickness, 0.4 mm Al added filtration, 9 collimator holes of 3 mm in size spread over 50 cm, 10 cm collimator thickness, 45 cm SAD, and 120° treatment arc. Next, for each investigated parameter, its values were varied according to Table I, while all the other parameters were kept at default and the KVAT dose distributions were evaluated using two metrics. The x-ray source output was evaluated by means of the dose delivered to 50% of the target volume in 30 min (D_{50}) and the spread of dose to healthy tissue was assessed by means of the target-to-skin ratio. The dose delivered to 50% of the target volume (D_{50}) was considered as the target dose. The D_{50} prescription dose was chosen to most readily compare to radiosurgical dosing and parallel Gamma Knife prescriptions. The skin dose was calculated as the mean dose to a (2 × 2) cm^2 area of the first phantom voxel layer on the central axis.

Based on the parameter study, a set of optimized parameters was derived resulting in the maximum target-to-skin ratio while maintaining a clinically acceptable dose output of 18 Gy at D_{50} during a 30-min irradiation in the homogeneous phantom. In addition, dose to the lung phantom was calculated for treatment parameters achieving sufficient dose output and target-to-skin ratio while maintaining low dose to the ribs. These were compared to dose in the homogeneous phantom. Radiation delivery was prescribed based on dose-volume nomograms used for standard radiosurgery.[14] Dose was prescribed to the tumor with tolerance of the skin and normal surrounding structures being the critical determinants of the treatment plan.[15]

2.D. Patient study

MC KVAT dose distribution was also calculated for a patient case. A hypothetical pararenal target located 12 cm deep was delineated in CT images of a patient's abdomen. The pararenal target was of ellipsoidal shape with dimensions ranging from 1.4 cm (in the left-right direction) to 1.8 cm (in the superior-inferior direction) and with equivalent sphere diameter of 1.6 cm. A KVAT x-ray source to treat the target was designed and the KVAT dose distribution compared to a 15 MV dose distribution. Both dose distributions were normalized to D_{95} receiving 100% of prescription dose.

2.D.1. Patient modeling

In the interest of calculation time, CT images of the patient's abdomen with (0.78 × 0.78 × 5.0) mm^3 voxels were downsampled and converted into an MC.egsphant file with (3.1 × 3.1 × 5) mm^3 voxels using RT_Image.[16] CT numbers were converted into mass densities using a clinical calibration curve. In addition, four materials from the default 521 ICRU cross-section data file were assigned based on CT numbers using the following ranges: air [−1000:−950], lung [−950:−200], ICRU tissue [−200:200], and cortical bone [200:3000].

2.D.2. Patient dose calculations

Patient dose distributions for 200 kV KVAT were calculated with MC simulations. The 200 KVAT treatment source was optimized based on the results of the phantom KVAT parameter study. More specifically, the electron beam energy was set to 200 keV, anode thickness to 32 μm, beam filtration to 0.4 mm Cu, number of collimator holes to 15, source extent to 45 cm, collimator hole size at the anode side to 4 mm, collimator thickness to 10 cm, and source-to-isocenter distance to 24 cm. Due to the more central location of the target, a treatment arc of 360° was selected. Note that a clearance of 4 cm between the patient's skin and the source was ensured, since the target was located at a maximum depth of 20 cm.

The dose to the target was also calculated for a 15 MV VMAT treatment in Eclipse (version 11, Varian Medical, Palo Alto, CA). The Eclipse dose was calculated for a single arc using the standard TrueBeam multileaf collimator (120 MLC) with the analytical anisotropic algorithm (AAA).

The 200 kV KVAT and 15 MV VMAT plans were normalized to 100% of prescription dose to cover 95% or the target volume and compared by means of the new conformity index (CI) defined as:

$$CI = \frac{TV \times PIV}{(TV_{PIV})^2},$$

where TV is the target volume, PIV is the volume encompassed by the prescription isodose line and TV_{PIV} is the target volume encompassed by the prescription isodose line.[17] In addition, CL_x was used to compare the volumes receiving a dose of interest of at least x% of the prescription dose calculated as:

$$CI_x = \frac{V_x}{TV},$$

where V_x is the volume receiving at least x% of the prescription dose. In order to compare KVAT and VMAT dose distributions for lower dose levels, CI_{50}, CI_{30}, and CI_{10} were investigated.

3. RESULTS

The principle of KVAT dose delivery to a deep-seated target, as well as the results for phantom KVAT source parameter study and optimum phantom and patient dose calculations, are presented below.

3.A. KVAT dose distributions

Dose distributions delivered with 200 kV x-ray beams to the 4-cm diameter target at 10-cm depth in a 40-cm

diameter cylindrical phantom using various beam arrangements and leading to a conformal KVAT dose are presented in Fig. 3. Note that, unless stated otherwise, the dose distributions are calculated with the default parameters listed in Table I. In Fig. 3(a), the dose distribution for a single 200 kV beamlet is presented. It is clear that the beam was not sufficiently penetrating and the target dose was less than 10% of the maximum dose that was deposited in the skin. The dose distribution for nine stationary beamlets is presented in Fig. 3(b). The maximum dose (D_{max}) occurred in the skin, but thanks to the contribution of the lateral beamlets, the dose to the target increased to 30% of D_{max}. For a 120° arc treatment (Fig. 3(c)), the nine beamlets generated a dose distribution where D_{max} shifted from the skin to the target, the skin dose decreased to 50% of D_{max} and the target dose increased to 70% of D_{max}. When increased beam weighting was applied to peripheral beamlets (Fig. 3(d)), the skin dose decreased further to 30% and the target dose increased to 80% of D_{max}. Beamlet weighting was implemented to counteract the effect of inverse square law due to the increased distance of the beamlets to the target.

3.B. Parameter study

The effects of electron beam energy, anode thickness, and beam filtration on x-ray energy spectra calculated from phase-space files scored just below the collimator are shown in Fig. 4. As expected, increasing the electron beam energy increased the mean spectrum energy (from 54.8 to 69.2 keV) and the x-ray beam output (from 5.2×10^{-8} to 1.8×10^{-7} x-rays/incident electron). When tungsten anode thickness was increased from 12 to 32 μm, the x-ray beam mean energy moderately increased (from 66.4 to 74.4 keV), while the x-ray beam output moderately decreased (from 1.9×10^{-7} to 1.5×10^{-7} x-rays/incident electron). X-ray beam filtration most affected the x-ray beam mean energy and output. When the beam filtration was increased from 0.4 mm Al to 3 mm Cu, the x-ray beam mean energy increased from 69.2 to 122.9 keV and the x-ray beam output decreased significantly from 1.8×10^{-7} to 2.1×10^{-8} x-rays/incident electron. It was therefore expected that x-ray beam filtration would have the largest effect on both studied KVAT dose distribution metrics, the x-ray beam output expressed by D_{50} in 30 min and the target-to-skin ratio.

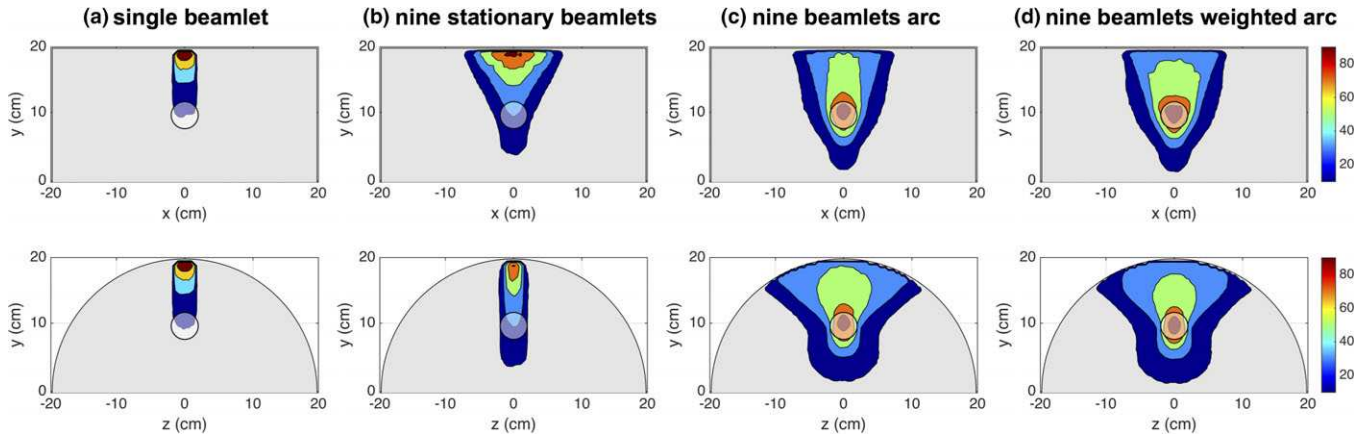

FIG. 3. Sagittal (top row) and axial (bottom row) view of dose distributions calculated for 200 kV beams using a number of beam arrangements. Single beamlet (a), nine stationary beamlets (b), a 120° arc delivery with nine beamlets (c) and the same 120° arc delivery with increased beam weighting for peripheral beamlets. Color bar presents percentage of D_{max}. [Color figure can be viewed at wileyonlinelibrary.com]

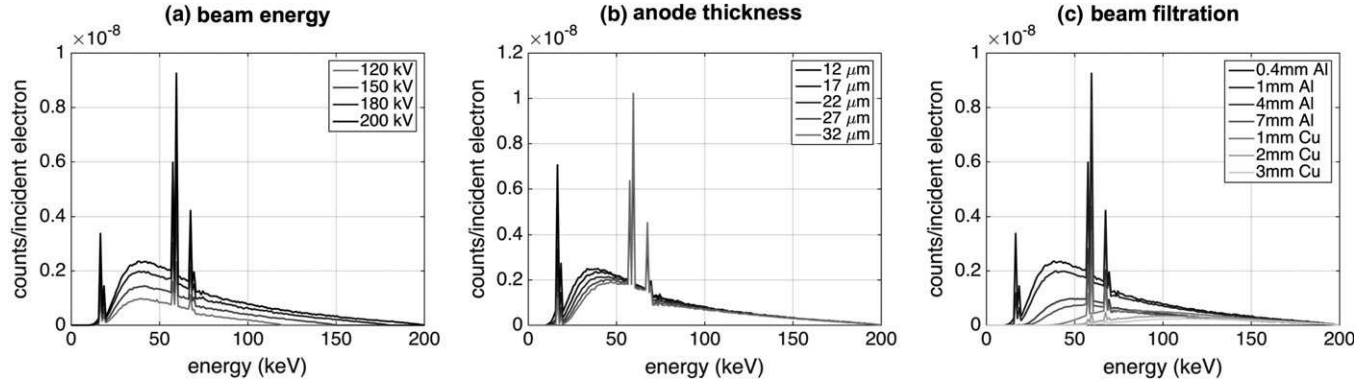

FIG. 4. Energy spectra scored below the collimator of beams generated with the default parameters (Table I) for varying beam energy (a), anode thickness (b), and added filtration (c).

The energy fluence plots of combined phase-space files containing all beamlets for a number of studied source parameters are shown in Fig. 5. The effect of electron beam energy, target thickness, beam filtration, number of collimator holes, collimator hole size at the target side, and collimator thickness on x-ray beam output and beamlet spatial distribution can be visualized. The energy fluence of the x-ray beam was the most affected by electron beam energy, filtration, and collimator hole size and thickness. The total energy fluence was increased by a factor of 4.5 when the electron beam energy was increased from 120 to 200 keV and when beam filtration was reduced from 3 mm Cu to 0.4 mm Al. The total energy fluence was increased by a factor of 2.5 when the collimator thickness was reduced from 12 cm to 6 cm and the collimator hole size was increased from 1 to 7 mm. Target thickness reduced the energy fluence by less than 20% for the two extreme cases of 12 μm and 32 μm. When the number of collimator holes was increased from 7 to 21, the x-ray beam spread over a larger area, but the total energy fluence remained constant. The energy spectrum and fluence plots can be utilized to guide the KVAT source optimization study.

A summary of the effect of all studied parameters on D_{50} in 30 min and target-to-skin ratio is presented in Fig. 6. In order to generate the highest output source with the highest skin sparing effect, both functions should be maximized in the design of an optimal KVAT x-ray source. As seen in Fig. 6, when D_{50} in 30 min increases, target-to-skin ratio decreases, or vice versa, for most studied KVAT x-ray source and treatment parameters. Therefore, a compromise resulting in a high quality dose distribution with a satisfactory output was sought.

As expected, the D_{50} in 30 min and target-to-skin ratio both increase with increasing electron beam energy and decreasing SAD. As a result, the x-ray beam energy should be maximized and SAD minimized in an optimal KVAT x-ray source. When the beam filtration of the KVAT x-ray source increased from 7 mm Al to 1 mm Cu, the target-to-skin ratio increased by 35% while the output remained constant. Beam filtration, treatment arc and beam energy had the largest effect on the output of the KVAT x-ray source. On the other hand, target-to-skin ratio was most affected by collimator hole size, beam filtration, and SAD. Interestingly, the studied number of collimator holes had a negligible effect on both metrics when KVAT x-ray sources with 7 to 21 collimator holes were modeled.

3.C. Phantom dose calculations

Based on the results presented in Fig. 6, the following source and treatment parameters were selected to generate an optimized KVAT dose distribution for a 4-cm diameter target at 10-cm depth in a 40-cm diameter phantom. These parameters were considered sufficiently challenging to adequately evaluate the performance of the kilovoltage source. The electron beam energy was set to 200 keV, anode thickness to 32 μm, beam filtration to 0.4 mm Cu, number of collimator

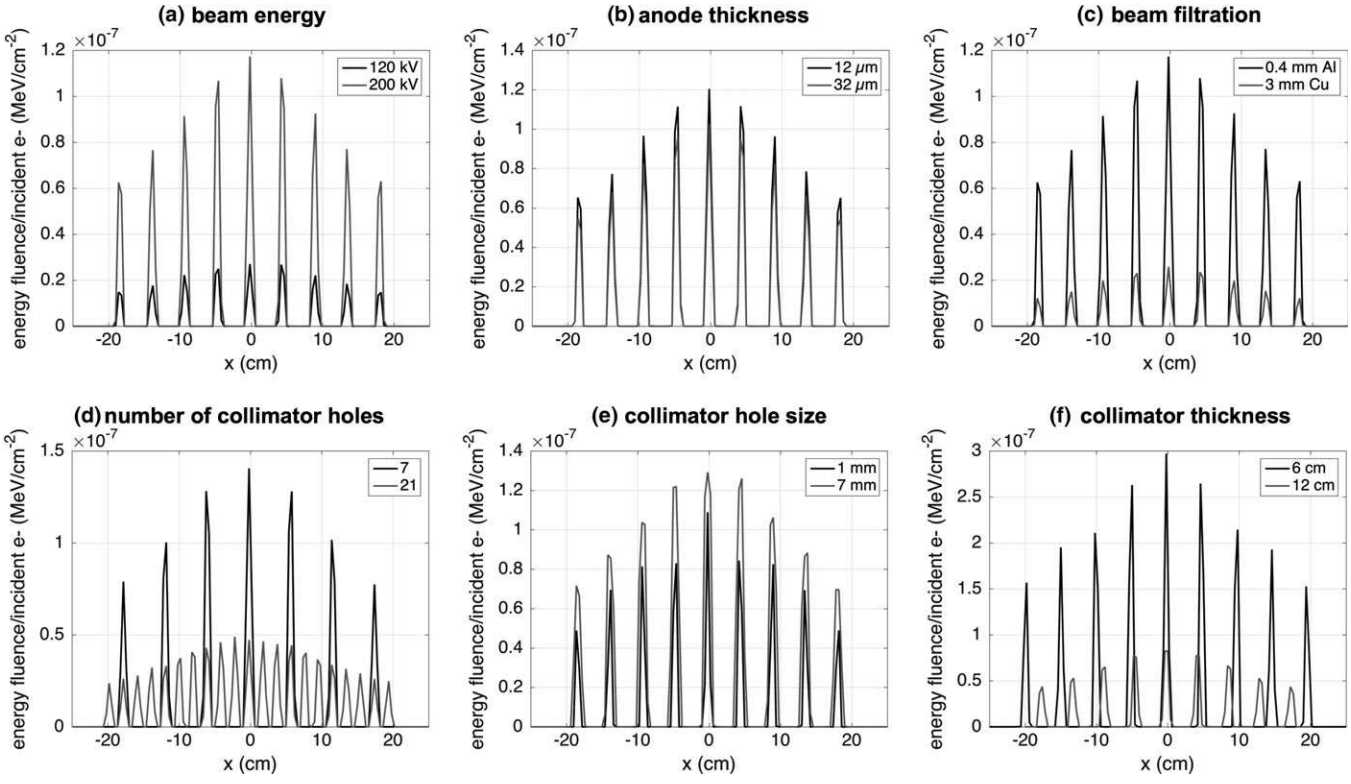

FIG. 5. Energy fluence as a function of distance scored below the collimator for x ray source geometry with the default parameters (Table I) but with varying beam energy (a), anode thickness (b), added filtration (c), number of collimator holes (d), collimator hole size (e), and collimator thickness (f).

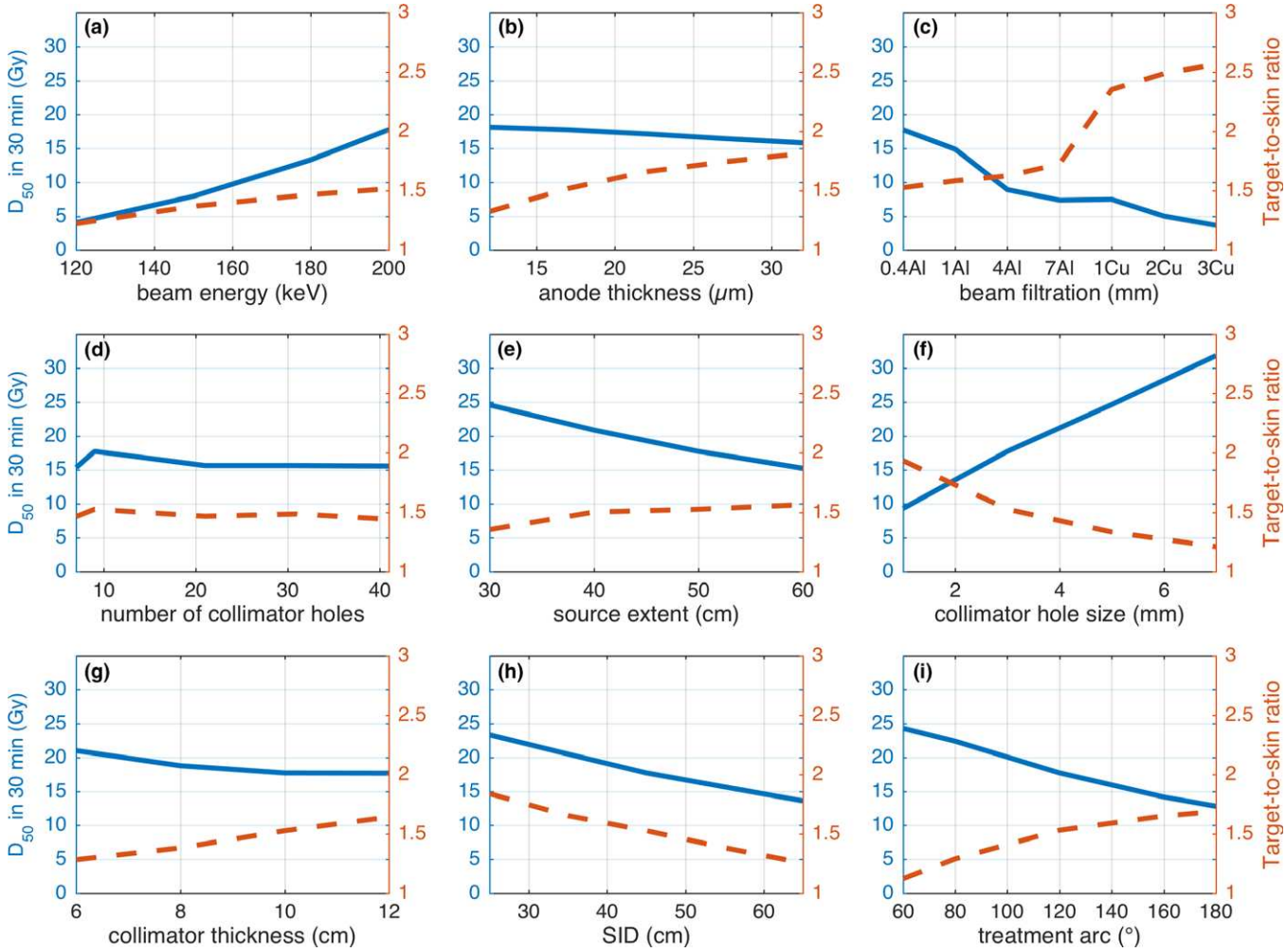

FIG. 6. D_{50} in 30 min (solid line) and target-to-skin ratio (dashed line) as a function of beam energy (a), anode thickness (b), beam filtration (c), number of collimator holes (d), source extent (e), collimator hole size (f), collimator thickness (g), source-to-isocenter distance (h), and treatment arc (i). [Color figure can be viewed at wileyonlinelibrary.com]

holes to nine, source extent to 60 cm, collimator hole size at the anode side to 5 mm, collimator thickness to 10 cm, SAD to 20 cm, and treatment arc to 120°. Beamlet weighting was implemented so that the skin dose for all beamlets was within 10%. The optimized dose distribution in the phantom is presented in Fig. 7. All three orthogonal views are shown, as well as the depth dose along the central axis of the KVAT source ($x = 0$ cm and $z = 0$ cm), the beam profiles across the center of the target, and the target dose-volume histogram (DVH).

Due to the higher beam energy as a result of the optimization, the skin dose was significantly decreased with a target-to-skin ratio of 5.1 and a D_{50} in 30 min of 24.1 Gy. The dose distribution was moderately conformal with a steep dose fall-off in the plane perpendicular to the beam direction; moreover, the target dose was non-uniform, as seen in the depth dose curve. The minimum and maximum target dose was 45% and 141% of D_{50}, respectively.

Dose distributions calculated for a 200 kV beam filtered with 1.0 mm Cu in the homogeneous and lung phantoms are presented in Fig. 8. The dose in the lung phantom was more conformal with higher dose to the target and higher target-to-skin ratio compared to the dose in the homogeneous phantom (Table II, right column). D_{50} and target-to-skin ratio in the lung phantom increased by 34% and 42%, respectively, compared to the homogeneous phantom. The maximum dose to the ribs in the lung phantom was 33% of D_{max} (= 36.0 Gy), but only 3% of the rib volume was irradiated to doses higher than 10 Gy. The dose to ribs was increased by a factor of 2 with respect to dose in the same location in the homogeneous phantom.

The dose distribution in the homogeneous phantom irradiated by the 200 kV beam filtered with 1.0 mm Cu was more conformal than the dose distribution calculated with the 200 kV beam filtered with 0.4 mm Cu (Table II), albeit with lower dose to the target. Data presented in Table II further show that in the homogenous phantom with the increased Cu filter thickness, D_{50} delivered in 30 min decreased by 22% and the target-to-skin ratio moderately increased by 4%. Similarly, Table II demonstrates a 29% decrease in D_{50} in

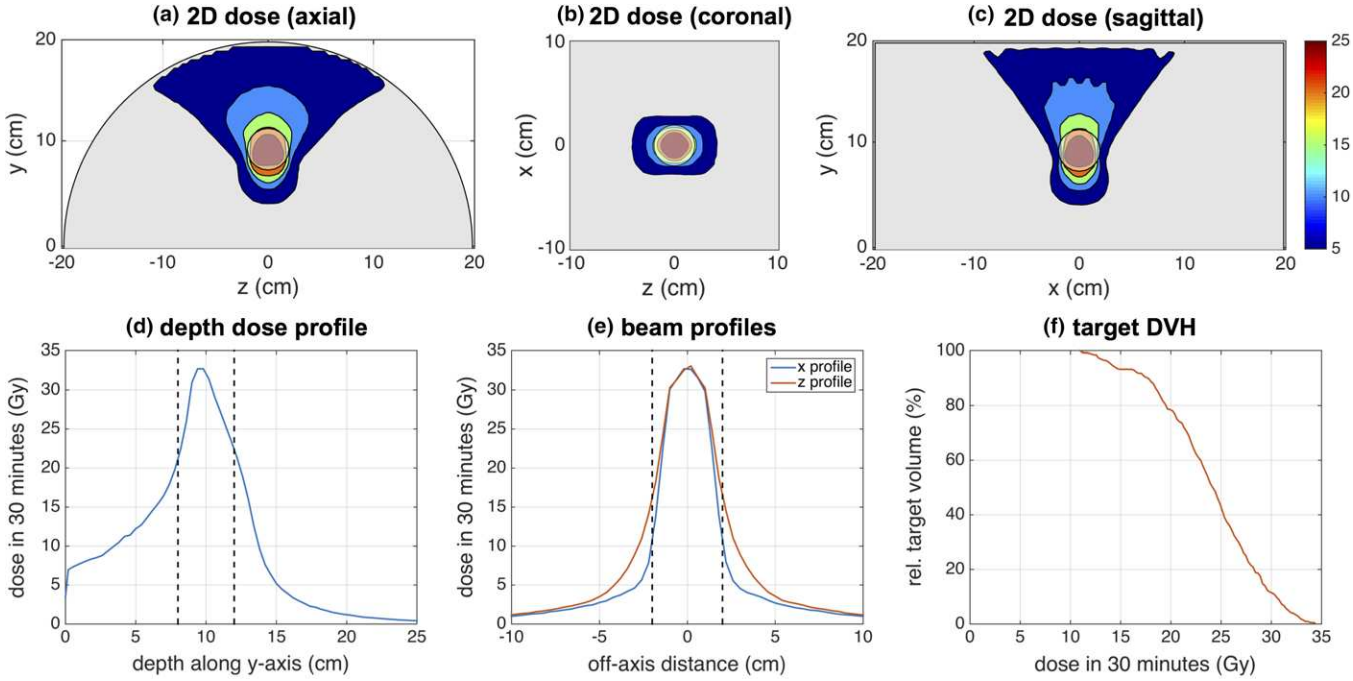

FIG. 7. Optimized dose distributions in the homogeneous phantom in the axial (a), coronal (b), and sagittal (c) views through the center of the spherical target calculated for a 200 kV beam filtered with 0.4 mm Cu. Dose profiles along the *y*-axis (d) and along the *x*- and *z*-axis (e) with target location shown by the dashed line. DVH of the target is shown in (f). All doses are shown in Gy and normalized to dose delivered in 30 min. [Color figure can be viewed at wileyonlinelibrary.com]

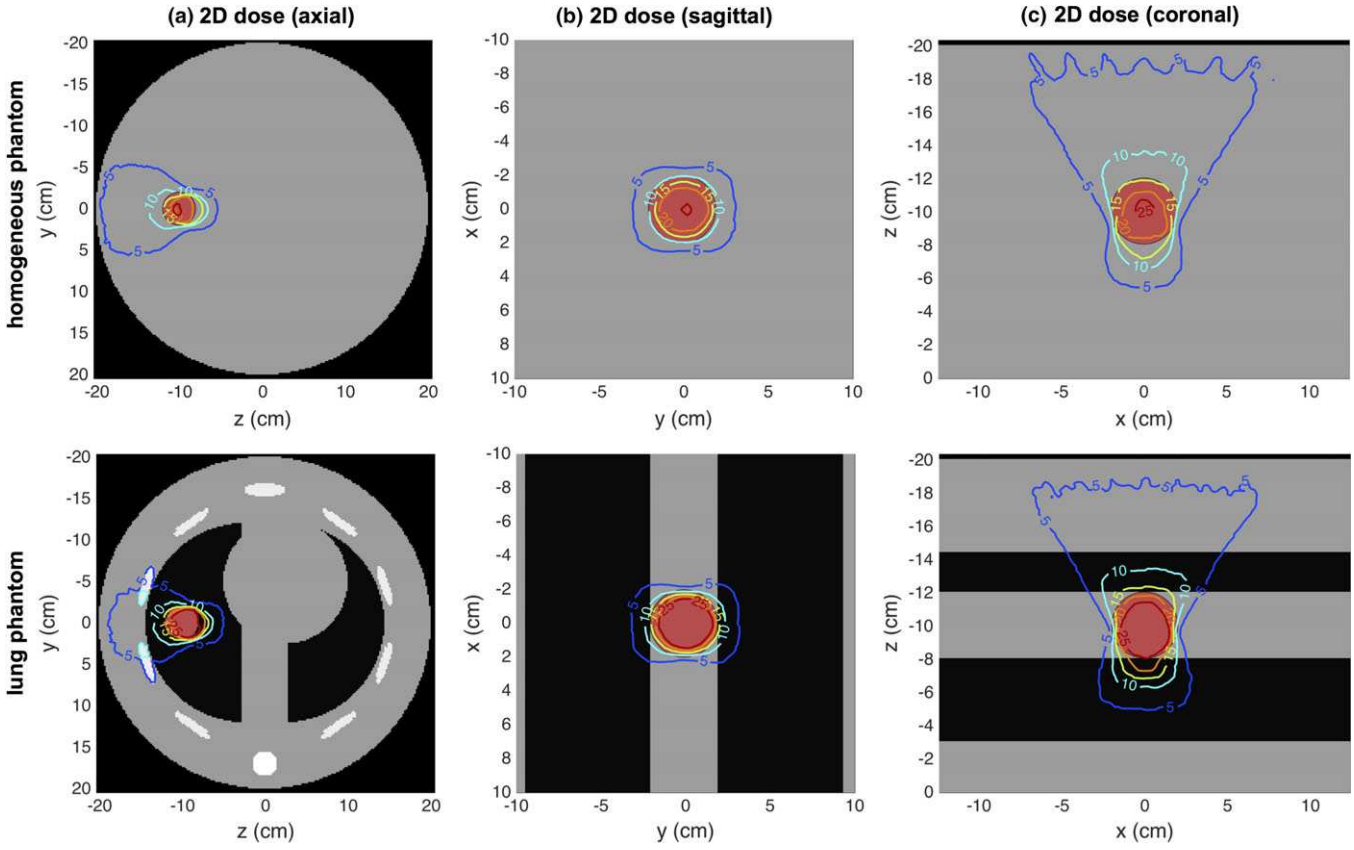

FIG. 8. Dose distributions calculated for a 200 kV beam filtered with 1.0 mm Cu in the axial (a), sagittal (b), and coronal (c) views plotted through the center of the target for a homogeneous phantom (top row) and a lung phantom (bottom row). Isodose lines are shown in Gy and represent dose delivered in 30 min. [Color figure can be viewed at wileyonlinelibrary.com]

TABLE II. X ray output expressed as D_{50} in 30 min and target-to-skin ratio for the 200 kV beam filtered with 0.4 mm Cu and 1.0 mm Cu for the homogeneous as well as lung phantom.

	200 kV with 0.4 mm Cu		200 kV with 1.0 mm Cu	
	Homogeneous	Lung	Homogeneous	Lung
D_{50} in 30 min (Gy)	24.1	35.4	18.9	25.3
Target-to-skin ratio	5.1	4.4	5.3	7.5

30 min and 70% increase in target-to-skin ratio for the heterogeneous phantom dose calculations with increased Cu filtration.

3.D. Patient dose calculations

For the patient CT-based calculations, the 200 kV KVAT and 15 MV dose distributions, as well as DVHs for the target and organs at risk (OARs), are presented in Fig. 9. The dose fall-off outside of the target was slower for the 200 kV KVAT dose distribution than for the 15 MV VMAT dose distribution, which was also demonstrated by the higher 200 kV KVAT body dose represented in the DVH plot. The 200 kV KVAT and 15 MV VMAT body mean dose was 2.0% and 0.4% of the prescription dose, respectively, which in either case, would be a fraction of the radiation dose from a single treatment in a conventional, multiweek regimen, and thus was of little clinical impact.

The presented 200 kV KVAT dose distribution resulted in a similarly uniform target dose compared to the 15 MV VMAT dose distribution. The target was fully covered by the 99% isodose line in both dose distributions and the maximum target dose was 108% and 105% of the prescription dose for the 200 kV KVAT and 15 MV VMAT dose distribution, respectively.

The target and OARs mean and maximum doses are listed in Table III. All OAR mean doses for both modalities were less than 10% of the prescription dose. With the exception of spleen and liver with <1% of prescription dose in the VMAT plan, KVAT OAR mean doses were on average about 80% higher than VMAT OAR doses. The maximum doses for OARs were similar for both modalities, with a higher maximum VMAT dose to the aorta (40.6% compared to 31.1% for KVAT) and higher maximum KVAT dose to the spleen (7.0% compared to 0.5% for VMAT).

The new conformity index CI was 1.2 for both the 200 kV KVAT and 15 MV VMAT dose distribution, further demonstrating comparable conformity of the two plans. All CI indices are presented in Table IV. While CI_{50} was comparable for the two plans, CI_{30} and CI_{10} were higher in the 200 kV KVAT plan than in the 15 MV VMAT plan, indicative of the higher volume irradiated to low doses by the 200 kV KVAT source.

4. DISCUSSION

Phantom dose calculations demonstrated that a 4-cm target at 10-cm depth could be treated with multi-focal-spot kilovoltage x-rays to a dose of 24.1 Gy with a satisfactory target-to-skin ratio of 5.1. In this case, dose was prescribed so as not to exceed tolerance of the skin, for example, 5 Gy[15] while

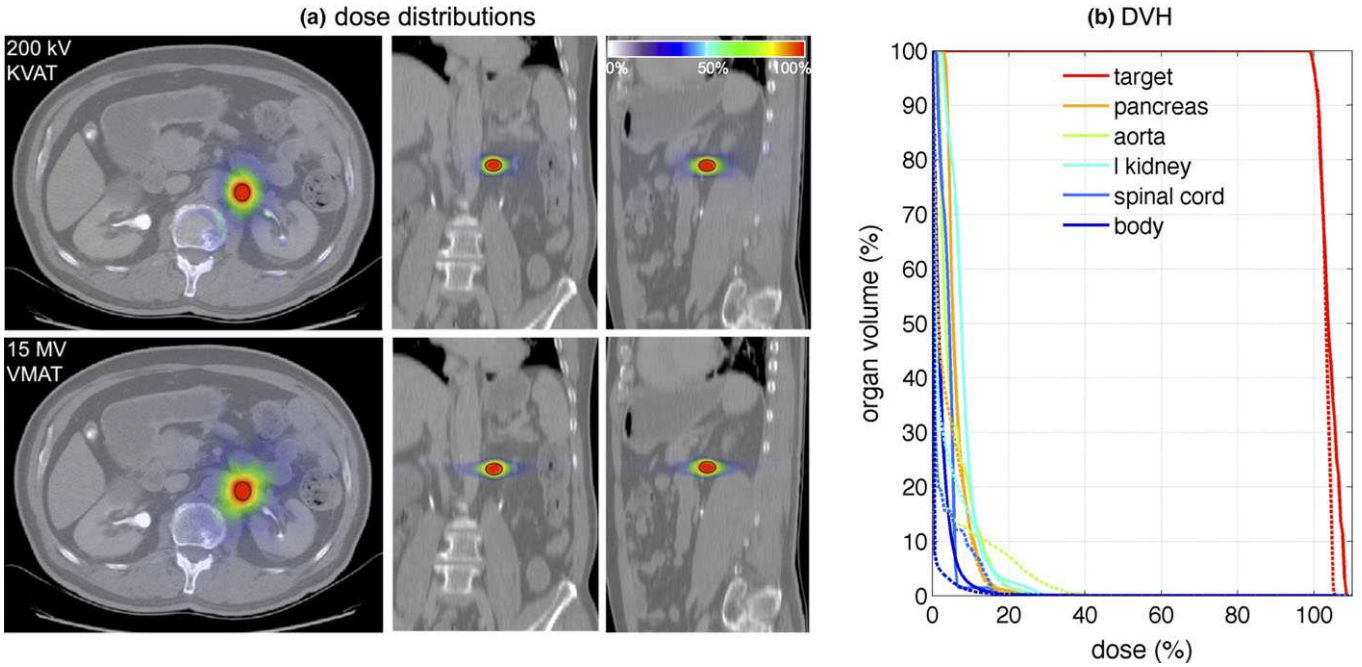

FIG. 9. Patient dose distributions (a) for 200 kV KVAT (top) and 15 MV VMAT (bottom) treatments of the left pararenal lesion. Target and body dose-volume histograms for the kilovoltage and megavoltage dose distributions are shown in (b). The 100% isodose line in the 200 kV KVAT irradiation corresponds to a dose of 20 Gy delivered in 30 min. [Color figure can be viewed at wileyonlinelibrary.com]

TABLE III. Target and OAR mean and maximum organ doses for the 200 kV KVAT and 15 MV VMAT dose distributions. All doses are represented as the percentage of prescription dose.

		Target	Left kidney	Pancreas	Aorta	Spinal cord	Spleen	Right kidney	Liver	Body
Mean dose (%)	200 kV	103.7	8.1	6.5	5.6	4.1	3.1	2.4	2.4	2.0
	15 MV	102.7	3.3	3.7	3.2	1.9	0.1	1.4	0.6	0.4
Max dose (%)	200 kV	108.0	39.0	32.7	31.1	17.2	7.0	9.2	32.7	108.0
	15 MV	105.0	36.2	33.0	40.6	15.5	0.5	9.9	33.0	105.0

TABLE IV. CI indices for pararenal lesion dose calculations.

	CI	CI_{50}	CI_{30}	CI_{10}
200 kV	1.2	10.5	28.3	411.7
15 MV	1.2	9.4	24.8	186.4

delivering a lethal tumor dose based on radiosurgical nomograms for the given tumor volume.[14] Prescription to the 50% isodose line was employed assuming the prospective use of such a device would be exclusively ablative (in the radiosurgical meaning of the term). We used D_{50} at 30 min as our output metric. In most cases that dose exceeds required minimum dosing for a given tumor volume. As such, clinical prescriptions to a lesion would be for less dose, and never exceed skin tolerance. It is worth noting that delivery of radiosurgical dosing over 30 min might permit significantly more patients to be treated at a facility on a monthly basis. In the design of the KVAT x-ray source, the beam energy, beam filtration, collimator hole size, source-to-isocenter distance, and treatment arc had the largest effect on the source output and the quality of dose distributions. Note that the KVAT source optimization dose calculations were somewhat limited, since the phantom was modeled as a homogeneous cylinder.

The lung phantom dose calculations demonstrate decreased attenuation in the lungs compared to soft tissue, as well as increased attenuation and elevated dose in the bony structures. The elevated dose to bony structures could possibly be prevented if the beam angles resulting in rib dose are avoided. The lung phantom dose calculation emphasizes the need for an inverse treatment planning for KVAT.

The patient dose calculations showed that high conformity in a small ~1.6-cm diameter regularly shaped target located deep in a patient's body could be achieved with the proposed KVAT source. Conformity indices for lower dose levels revealed that the volumes irradiated by at least 50% of the prescription dose were comparable in the 200 kV KVAT and 15 MV VMAT plans. However, the volume irradiated by at least 10% of the prescription dose was a factor of 2.2 larger in the 200 kV KVAT dose distribution compared to the 15 MV VMAT plan. While the effects of low doses of radiation have not been consistently described, the 10% dose level described here is in the range of a single radiation fraction used in a conventional 6-week course of daily radiotherapy. The larger low-dose volume will be in future work better optimized for the clinical usage of the proposed KVAT x-ray source.

Compared to the phantom 4-cm target dose distributions, KVAT target conformity was improved for the smaller regular pararenal target. Treatments of complex targets could be done with a CyberKnife- or Gamma Knife-like approach of "packing spheres or shots."[18] As in the original version of the CyberKnife, where a number of fixed collimators were employed, the KVAT source could be designed with a number of varied collimator sizes in order to accommodate treatments of different target sizes. An analogous approach was implemented to generate a line distribution in the work by Prionas et al.[3]

Kilovoltage x-ray beam dose distribution is affected by tissue heterogeneities to a higher degree than megavoltage beam radiotherapy, that is, higher attenuation, as well as higher dose to bony tissues, due to the increased probability of photoelectric interactions. The patient dose distribution in Fig. 8 a demonstrated this effect. The maximum dose to the bony spine was 35% and 22% of the prescription dose in the 200 kV KVAT and 15 MV dose distribution, respectively. Further optimizing the KVAT source in terms of beam energy and filtration could reduce bone dose.

In order to perform radiotherapy of deep-seated targets with the proposed KVAT x-ray source, the energy of the original 120 kV imaging source was increased to 200 kV while maintaining the tube current of 200 mA. As a result, the power requirements increased by 67% and a 40 kW power supply would be necessary to power the therapy x-ray source. Heat dissipation will become important to the KVAT x-ray source design; however, larger number of beamlets would mitigate overheating.

A key to understanding the concept presented here is the multi-focal-spot nature of the device. For this application, that property has an important implication on the distribution of heat. Heat is spread over a large anode area with the same beneficial effect as in a rotating-anode tube, for example, for CT or angiography. The 120 kV source mentioned above is able to put such a high heat load through its anode because of the area of the anode illuminated and because each beamlet is generated sequentially, allowing the anode to cool in that location will other locations are illuminated. Finally, we note that while, as illustrated in Fig. 6, the number of collimator holes (equal to the number of focal spots) has negligible impact on the two figures of merit plotted, a larger number of holes/spots can have a substantial impact on the question of heat loading. This represents a design degree of freedom, the

optimization of which remains for the engineering effort of source development.

A kV therapy source obviates the requirement of a concrete vault with 2-meter thick walls for adequate shielding. As such, an "out-of-the-bunker" system saves $1.5M in facility construction costs. Aside from the lower cost of the KVAT x-ray source, which we estimate to be approximately 10% of the least costly conventional radiotherapy systems,* another advantage of the KVAT x-ray source could be the possibility to perform imaging just prior and during treatment. Our future work will include studies of KVAT x-ray imaging during radiotherapy as well as investigations of KVAT treatments of targets of various sizes, shapes, and depths.

5. CONCLUSIONS

A Monte Carlo model of a novel kilovoltage arc therapy (KVAT) x-ray source has been built and optimized for treatments of a 4-cm diameter target. We have demonstrated that the KVAT x-ray source could deliver a 24.1 Gy dose to the target located at 10-cm depth in a 40-cm diameter cylindrical phantom during a 30-min irradiation with a sufficient target-to-skin ratio of 5.1. In addition, a 200 kV KVAT dose delivered to a patient's pararenal lesion was comparable in terms of target conformity compared to a 15 MV VMAT plan. However, the volume irradiated to at least 10% of the prescription dose was larger in the 200 kV KVAT plan than in the 15 MV VMAT plan. This work serves as a proof-of-principle study demonstrating the feasibility of irradiating a deep-seated spherical target with a 200 kV beam.

ACKNOWLEDGMENT

We would like to thank Dr. Larry Partain of TeleSecurity Sciences for valuable discussions on the design of the presented KVAT source. This work was partly supported by Sirius Medicine, LLC, and the Natural Sciences and Engineering Research Council of Canada.

CONFLICT OF INTEREST

Michael D Weil is the founder of Sirius Medicine, LLC, who in part financially supported this work.

[a)]Author to whom correspondence should be addressed. Electronic mail: bazalova@uvic.ca.

REFERENCES

1. Morgan MA, Ten Haken RK, Lawrence TS., *Essentials of Radiation Therapy*, 10th ed. (Cancer: Principles & Practice of Oncology). Philadelphia: Lippincott Williams & Wilkins 2015.
2. Karzmark C. Advances in linear accelerator design for radiotherapy. *Med Phys*. 1984;11:105–128.
3. Prionas ND, McKenney SE, Stern RL, Boone JM. "Kilovoltage rotational external beam radiotherapy on a breast computed tomography platform: a feasibility study. *Int J Radiat Oncol Biol Phys*. 2012;84:533–539.
4. Van Lysel MS, Solomon EG, Wilfley BP, Dutta A, Speidel MA. Performance assessment of the scanning beam digital X-ray (SBDX) system. *Proc SPIE –Int Soc Opt Eng*. 1997;3032:161–170.
5. Ipton MJ, iggins CB, Boyd DP. Computed tomography of the heart: evaluation of anatomy and function. *J Am Coll Cardiol*. 1985;5:55S–69S.
6. Fryar CD, Gu Q, Ogden CL. Anthropometric reference data for children and adults: United States, 2007-2010. *Vital Health Stat 11, Data From the National Health Survey*. 2012;252:1–48.
7. Edge SB, Compton CC. The American Joint Committee on Cancer: the 7th edition of the AJCC cancer staging manual and the future of TNM. *Ann Surg Oncol*. 2010;17:1471–1474.
8. Kawrakow I, Rogers DWO. *The EGSnrc Code System: Monte Carlo Simulation of Electron and Photon Transport*. ed: NRCC 2006.
9. Rogers DWO, Walters B, Kawrakow I. *BEAMnrc Users Manual*. ed: NRCC 2006.
10. Ali ESM, Rogers DWO. Efficiency improvements of x-ray simulations in EGSnrc user-codes using bremsstrahlung cross-section enhancement (BCSE). *Med Phys*. 2007;34:2143–2154.
11. Walters BRB, Kawrakow I, Rogers DWO. *DOSXYZnrc Users Manual*. ed: NRCC 2007.
12. Bazalova M, Weil MD, Wilfley B, Graves EE. Monte Carlo model of the scanning beam digital x-ray (SBDX) source. *Phys Med Biol*. 2012;57:7381–7394.
13. White D, Booz J, Griffith R, Spokas J, Wilson I. Tissue substitutes in radiation dosimetry and measurement. *ICRU Report*. 1989;44.
14. Weil MD. Stereotactic radiosurgery for brain tumors. *Hematol Oncol Clin North Am*. 2001;15:1017–1026.
15. Emami B, Lyman J, Brown A, et al. Tolerance of normal tissue to therapeutic irradiation. *Int J Radiat Oncol Biol Phys*. 1991;21:109–122.
16. Graves EE, Quon A, Loo BW. RT_Image: an open-source tool for investigating PET in radiation oncology. *Technol Cancer Res Treat*. 2007;6:111–121.
17. Paddick I. A simple scoring ratio to index the conformity of radiosurgical treatment plans: technical note. *J Neurosurg*. 2000;93:219–222.
18. Dieterich S., Gibbs I. C., The CyberKnife in clinical use: current roles, future expectations. In *IMRT, IGRT, SBRT*, vol. 43: Karger Publishers, 2011, pp. 181–194.

*M. Weil, *private communication*.